



Techniques for Estimations of Beam Energy Loss in the Two-beam Test Stand PETS, applied to the First 12 GHz PETS Tests with Beam

Erik Adli, University of Oslo and CERN*

Abstract

We discuss various methods to estimate the beam energy loss in the Two-beam Test Stand PETS, using a constant parameter recirculation model, based on different permutations of the available instrumentation. The formulæ for the beam energy loss are presented, and the various estimation approaches are applied to a number of pulses logged during the 2008 run.

Geneva, Switzerland

May 17, 2009

*Work supported by the Research Council of Norway, the Swedish Research Council and the Wallenberg Foundation

This page is intentionally left blank.

Contents

1	Introduction	1
2	Particle energy loss in the PETS	3
2.1	Energy loss derived from the PETS integrated field	3
2.2	Energy loss derived from PETS output power	4
2.3	Analytic equivalence of $\langle U \rangle_E$ and $\langle U \rangle_P$ for pulses with constant beam intensity	5
2.4	Energy loss assuming perfect recirculation phase	6
2.5	Calculated energy loss for pulses with constant intensity	6
3	Energy loss estimations using BPM horizontal position measurements	8
4	Energy loss estimations using PETS forward power measurement and BPM intensity measurements	11
5	Energy loss estimations using BPM intensity measurements alone	13
6	Comparison between the three estimates	15
6.1	Comparison for the example pulse	15
6.2	Comparison for pulses without pulse shortening	16
6.3	Comparison for pulse with pulse shortening	16
6.4	Statistics	17
7	Conclusions	27
7.1	Recommendations for future work	27
8	Acknowledgements	27
	References	28

1 Introduction

At the end of 2008 the first 12 GHz CLIC Power Extraction and Transfer Structure (PETS) [1] was tested with beam in the Two-beam Test Stand (TBTS) [2] in the CLIC Test Facility 3 [3]. The PETS is equipped with a field recirculator for increased power production from a low current beam [4].

In [5] we have shown how a simple constant-parameter model of recirculation can reproduce, with good accuracy, the PETS output power using beam intensity readings only. In [6] it is further shown how models with variable parameters can be used to fit the power and phase for shortened pulses. In this note we discuss the beam energy loss in the TBTS PETS.

Studies of the beam energy loss in the PETS are important to verify the nominal performance of the PETS, to verify that the energy loss is consistent with the power production, to benchmark the theory and simulations, and as a tool to characterise break down. In this note we will primarily be concerned with nominal operation mode of the PETS and not in detailed break down studies.

Based on the available TBTS instrumentation as well as the system model presented in [5] we can estimate the beam energy loss using three separate measurement sets, using different approaches:

1. Estimation using horizontal BPM position measurements, including the dispersive section downstream of the PETS
2. Estimation using the PETS forward power measurements and the BPM intensity measurements
3. Estimation using the BPM intensity measurements alone, using the recirculation model to reconstructed PETS power

We will first develop a mathematical expression of the energy loss, using the model derived in [5]. Each estimation approach is then explained. Finally, we present the energy loss estimated with the three different approaches for a number of pulses, both with and without pulse shortening.

The notation used in this note is the same as defined in [5]. Table 1 summarises the quantities used in this note, including the relevant quantities discussed further in [5].

A sketch of the Two-beam Test Stand in its December 2008 configuration is depicted in Figure 1.

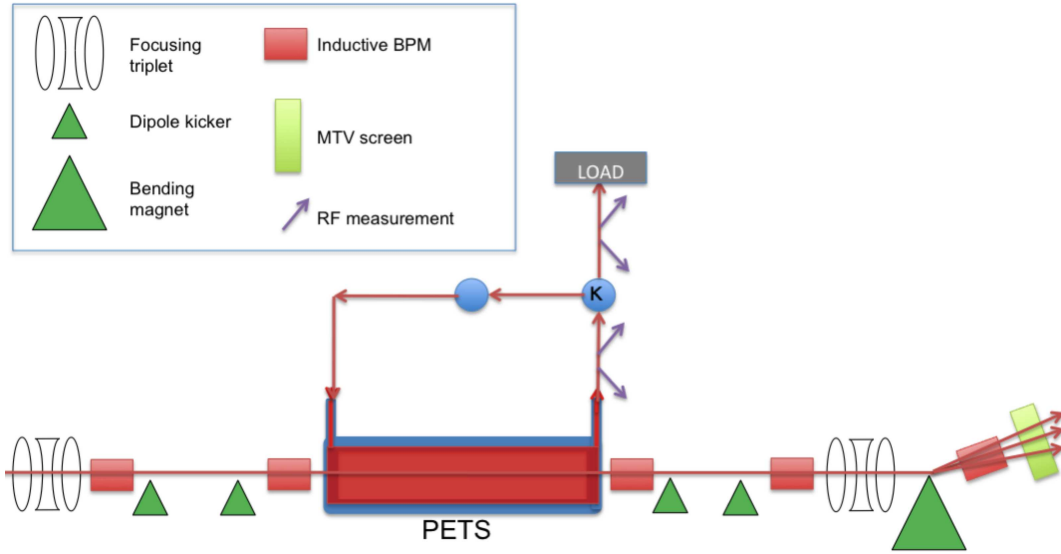


Figure 1: Sketch of the Two-beam Test Stand (not to scale) - December 2008 configuration

Quantity	Symbol	Value	Unit
PETS peak electric output field generated by the beam before recirculation starts to act	E_{beam}		V/m
PETS total peak output electric field (with recirculation)	E		V/m
PETS RF power output (with recirculation)	P		W
Voltage seen by a particle passing through the PETS	U		V
Charge distribution form factor	$F(\lambda)$		-
PETS ohmic losses reduction factor	$\eta_{\Omega, PETS}$	0.98	-
PETS active length	L	1	m
Beam pulse intensity	I		A
Total field recirculation gain after one round-trip	g	0.75	-
Recirculation phase-shift (phase-error)	ϕ	-18	deg
Horizontal BPM position reading	x		m
Horizontal dispersion	D		m
Relative momentum deviation along the pulse	$\delta \equiv \frac{\Delta p}{p_0}$		-

Table 1: Parameters relevant TBTS PETS energy loss estimations

2 Particle energy loss in the PETS

When a particle passes through the PETS it will lose, or eventually gain energy due to the PETS integrated electric field (voltage) it sees.

With our definitions positive voltage seen by the particle will induce particle energy loss, while negative voltage seen will correspond to particle energy gain. We choose to still use the term "energy loss" in this note since it corresponds to nominal PETS operation.

We denote the peak voltage seen by the beam by \hat{U} . The voltage seen by the beam, $\langle U \rangle$, corresponding to the beam centroid energy loss is then given by [5]

$$\langle U \rangle = \hat{U}F(\lambda) \quad (1)$$

Thus, 1 V of mean voltage seen by the beam corresponds to 1 eV of beam centroid energy loss.

2.1 Energy loss derived from the PETS integrated field

The particle will only be affected with the field component in phase with it. We will in this section continue the use of the simple sausage beam model described in [5], assuming perfect bunch phasing.

We define the part of the total field in phase with the beam generated field to be the real part of the complex field vector. In the case of no recirculation the PETS peak voltage seen is

$$\hat{U}_{beam} = \frac{1}{2}E_{beam}L$$

where the factor $\frac{1}{2}$ enters because the beam generated field builds up stepwise in the PETS [5].

With field recirculation the real part of the circulated field over the full length of the PETS is also seen by the beam

$$\hat{U}_{circ,M} = \Re(E_{circ,M})L$$

where $E_{circ,M}$ is the total field circulated into the PETS after M full recirculation cycles [5]

$$E_{circ,M} = \sum_{m=1}^M g^m \exp(jm\phi) \quad (2)$$

The total peak voltage seen by the beam is thus $\hat{U}_M = \hat{U}_{beam} + \hat{U}_{circ,M}$, which we can write using the expression of the total peak field at the PETS output after M full recirculation cycles, $E_M = \sum_{m=0}^M g^m \exp(jm\phi)$ [5]. Note that summation starts from 0 for E_M and from 1 for $E_{circ,M}$ in Eq. (2). The total expression for the peak voltage seen after M full recirculation turns is thus

$$\hat{U}_M = \hat{U}_{beam} + \hat{U}_{circ,M} = \Re(E_M)L - \frac{1}{2}E_{beam}L \quad (3)$$

For the energy loss discussion we will be interested in the mean voltage $\langle U_M \rangle$ rather than the peak voltage, because a BPM downstream the PETS will pick up a signal corresponding to the beam centroid motion, given by

$$\langle x + D \frac{\Delta p_{PETS}}{p_0} \rangle = \langle x \rangle - D \frac{q \langle U \rangle}{\mathcal{E}_0}$$

where D is the dispersion at the BPM location and \mathcal{E}_0 is the centroid energy of the incoming beam, here assumed to be uniform.

Combining Eqs. (1) and (3) we get the total expression for the mean voltage seen by the beam in the PETS

$$\langle U_M \rangle_E = \Re(E_M)LF(\lambda) - \frac{1}{2}E_{beam}LF(\lambda) \quad (4)$$

We use the suffix E to indicate that the energy loss calculation is derived from field considerations.

2.2 Energy loss derived from PETS output power

The energy loss can be calculated in an alternative and equivalent way, considering the PETS output power P . The power out of the PETS must equal the absolute power circulated back into the PETS + the absolute power generated by the beam. The power circulated back into the PETS we have defined as g^2 times the PETS output power one recirculation cycle earlier, where g is the total recirculation gain defined in [5]. The PETS output power after M full recirculation cycles can thus be expressed as

$$P_M = g^2 P_{M-1} + P_{beam,M} \quad (5)$$

where $P_{beam,M}$ is the power extracted from the beam after M full recirculation cycles.

The power extracted from the beam can also be written as

$$P_{beam,M} = \langle U_M \rangle I_M \eta_{\Omega, PETS} \quad (6)$$

where $\langle U_M \rangle$ is the mean voltage seen by the beam, corresponding to the energy loss of the beam centroid. Combining Eqs. (5) and (6) we can therefore express the mean voltage seen by the beam as

$$\langle U_M \rangle_P = \frac{1}{I_M \eta_{\Omega, PETS}} (P_M - g^2 P_{M-1}) \quad (7)$$

We use the suffix P to indicate that the energy loss calculation is derived from power considerations.

2.3 Analytic equivalence of $\langle U \rangle_E$ and $\langle U \rangle_P$ for pulses with constant beam intensity

We derived expressions for the centroid energy loss based on two different viewpoints yielding Eqs. (4) and (7). For completeness we will now show that these two expressions are indeed equal for pulses with constant beam intensity, I .

Using formulæ derived in [5] we develop Eq. (7). Using

$$P_M = v_g \frac{E_M^2}{(R'/Q)\omega_{RF}}$$

we get

$$\langle U_M \rangle_P = \frac{1}{I \eta_{\Omega, PETS}} \frac{v_g}{(R'/Q)\omega_{RF}} (\text{Abs}\{E_M\}^2 - g^2 \text{Abs}\{E_{M-1}\}^2)$$

By further substituting

$$E_M = E_{beam} \sum_{m=0}^M (g \exp(j\phi))^m \equiv E_{beam} \frac{1 - (g \exp(j\phi))^{M+1}}{1 - g \exp(j\phi)}$$

and

$$E_{beam} = \frac{1}{2} (R'/Q)\omega_{RF} \frac{L}{v_g} IF(\lambda)\eta_{\Omega, PETS}$$

we get

$$\langle U_M \rangle_P = \frac{1}{2} E_{beam} LF(\lambda) \left(\text{Abs} \left\{ \frac{1 - (g \exp(j\phi))^{M+1}}{1 - g \exp(j\phi)} \right\}^2 - g^2 \text{Abs} \left\{ \frac{1 - (g \exp(j\phi))^M}{1 - g \exp(j\phi)} \right\}^2 \right)$$

We develop Eq. (4) in a similar manner

$$\begin{aligned} \langle U_{E,M} \rangle &= \Re(E_M) LF(\lambda) - \frac{1}{2} E_{beam} LF(\lambda) \\ &= \frac{1}{2} E_{beam} LF(\lambda) \left(2\Re \left\{ \frac{1 - (g \exp(j\phi))^{M+1}}{1 - g \exp(j\phi)} \right\} - 1 \right) \end{aligned} \quad (8)$$

Furthermore, for any complex number $q = g \exp(j\phi) \neq 1$ one can easily show the algebraic equivalence

$$2\Re \left\{ \frac{1 - q^{M+1}}{1 - q} \right\} - 1 \equiv \mathbf{Abs} \left\{ \frac{1 - q^{M+1}}{1 - q} \right\}^2 - \mathbf{Abs}(q)^2 \mathbf{Abs} \left\{ \frac{1 - q^M}{1 - q} \right\}^2$$

using e.g. the Identity Theorem of Complex Analysis. We have therefore shown $\langle U_M \rangle_P \equiv \langle U_M \rangle_E$ and that the two ways of calculating the beam energy loss are equivalent, assuming our simple model.

2.4 Energy loss assuming perfect recirculation phase

For a perfect recirculation phase ($\phi = 0$) the energy loss Eq. (8) reduces to

$$\langle U_{M,\phi=0} \rangle = \frac{1}{2} E_{beam} LF(\lambda) \frac{1 + g(1 - 2g^M)}{1 - g} \quad (9)$$

which, in the case of steady state conditions $M \rightarrow \infty$, becomes

$$\langle U_{SS,\phi=0} \rangle = \frac{1}{2} E_{beam} LF(\lambda) \frac{1 + g}{1 - g} \quad (10)$$

2.5 Calculated energy loss for pulses with constant intensity

Figures 2 and 3 show the calculated beam energy loss corresponding to 5 A rectangular beam pulses assuming point-like bunches and nominal PETS parameters, calculated using Eq. (4) (in red) and Eq. (7) (in blue). The recirculator settings used in Figure 2 is $g=0.5$, $\phi=0$ (recirculating 50 % of the field with no phase error), and the settings

for Figure 3 is $g=0.75$, $\phi = -18^\circ$ (the recirculator settings for the 2008 TBTS run, as estimated in [5]). The beam pulse intensity is shown in magenta.

In these examples the beam pulse has passed the PETS after 700 ns. Eq. (7) is calculated only up to 700 ns; however, Eq. (4) is calculated also for the time after the beam has passed. In Figure 3 the voltage in the PETS turns negative after the beam has passed, due to the non-zero recirculation phase. A sufficiently small charge entering the PETS in this time window would thus be accelerated.

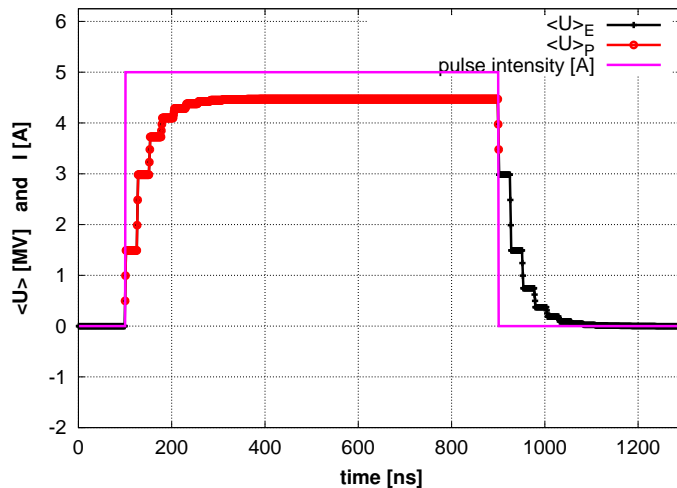


Figure 2: Calculation of beam energy loss in the TBTS PETS, using Eqs. (7) (red) and (4) (blue), for a rectangular pulse of 5 A (magenta). Recirculator settings are $g=0.5$ and $\phi=0$ deg

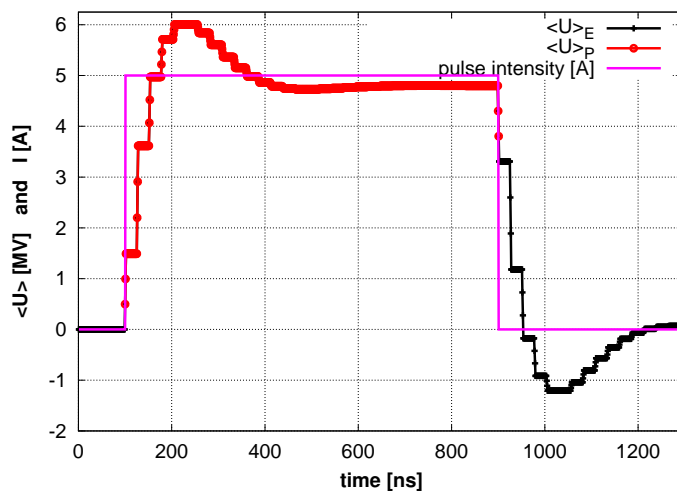


Figure 3: Calculation of beam energy loss in the TBTS PETS, using Eqs. (4) (blue) and (7) (red), for a rectangular pulse of 5 A (magenta). Recirculator settings are $g=0.75$ and $\phi=-18$ deg

3 Energy loss estimations using BPM horizontal position measurements

In this approach we use the least-squares method described in [7] to estimate $\delta \equiv \frac{\Delta p}{p}$. This method uses the horizontal position readings from all the 5 TBTS BPMs in order to estimate the parameter vector

$$\begin{bmatrix} x^1 \\ x'^1 \\ \theta \\ \delta \end{bmatrix} \quad (11)$$

where x^1 is the horizontal beam position in BPM 1, x'^1 the horizontal angle in BPM 1, θ the horizontal kick in the PETS and δ the energy loss in the PETS.

The estimation of δ is possible due to dispersion induced in the last BPM, CM.BPM0620, by the upstream bending magnet CM.BHB0620 ($D = 0.2$ m at the location of this BPM). Using the vertical BPM readings the vertical position, angle and kicks can be estimated as well. The locations of the five BPMs are shown in Figure 4.

The least-squares method allows for compensation of the incoming offsets and angles ¹ when estimating δ . This is necessary in order to estimate relative changes in δ along the pulse, because in the logged pulses both the incoming offset and the angle varies along the pulse, due to upstream beam dynamics effects.

We implement the least-square algorithm from [7] using matrix elements M_{ij}^{AB} retrieved from the TBTS MAD-X model [8], where \mathbf{M}^{AB} is the transfer matrix from position A to position B , and A and B refer to the longitudinal position of BPM 1 to 5, or to the position of the PETS kick and energy loss, K . We assume here that the kick and the energy loss take place in the middle of the PETS.

Estimation of Eq. (11) is performed by solving the following set of equations in the least-square sense

$$\begin{bmatrix} x^1 \\ x^2 \\ x^3 \\ x^4 \\ x^5 \end{bmatrix} = \begin{bmatrix} 1 & 0 & 0 & 0 \\ M_{11}^{21} & M_{12}^{21} & 0 & 0 \\ M_{11}^{31} & M_{12}^{31} & M_{12}^{3K} & 0 \\ M_{11}^{41} & M_{12}^{41} & M_{12}^{4K} & 0 \\ M_{11}^{51} & M_{12}^{51} & M_{12}^{5K} & M_{13}^{5K} \end{bmatrix} \begin{bmatrix} x^1 \\ x'^1 \\ \theta \\ \delta \end{bmatrix} \quad (12)$$

At this stage of the TBTS operation a precise knowledge of the precise BPM alignment was not available, and we will therefore consider only relative BPM offsets, and thus a relative change in δ along the pulse.

¹a discussion of the kicks estimated by this algorithm is planned in a future note

If the corrector coils in the TBTS are powered Eq. (12) has to be modified accordingly in order to estimate absolute parameter values, however, the corrector coil settings are irrelevant when estimating relative changes along the pulse.

To get the voltage in [V] we multiply δ with the best estimate of the CTF3 incoming beam energy, derived from the settings of the combiner ring, $\mathcal{E}_0 \approx 127$ MeV [9]. The voltage corresponding to the relative centroid energy loss is thus found as

$$\langle U \rangle_H [\text{V}] = -\delta \mathcal{E}_0 [\text{eV}] \quad (13)$$

where we use the suffix H to indicate estimations performed using the horizontal BPM readings.

Finally, it must be noted that for the TBTS 2008 run the energy profiles of the incoming pulses were not available. The energy change we estimate using the TBTS BPMs is thus the energy loss due to the PETS plus the relative energy variation of the incoming beam, $\delta = \delta_{PETS} + \delta_{incoming}$.

Figure 5 shows, in blue (x), the energy loss along the pulse estimated using the TBTS BPM horizontal readings, for the pulse denoted "example pulse" in [5]. As mentioned, the zero point of the ordinate axis depends on the absolute BPM position centre offsets, which are not known to precision at this stage of TBTS operation.

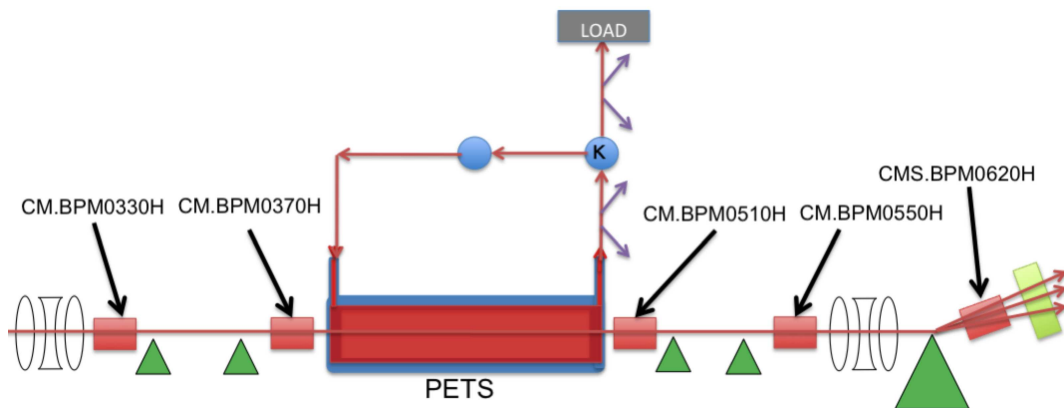


Figure 4: Location of the five BPMs used for estimating the beam energy loss in the TBTS PETS from BPM horizontal position measurements

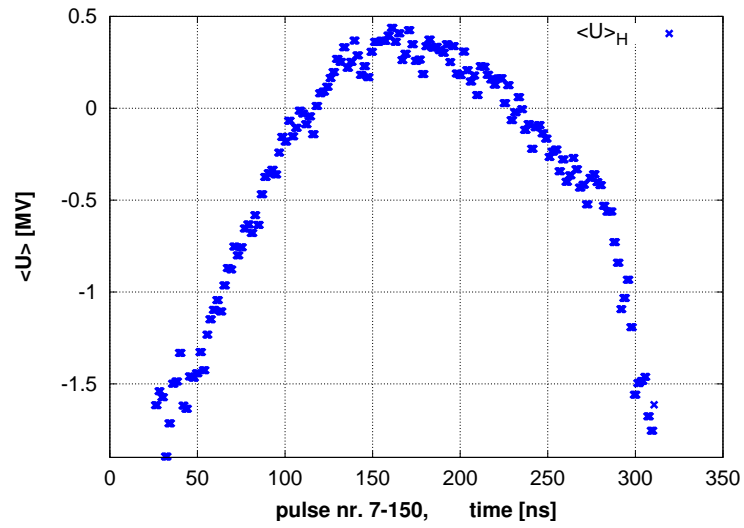


Figure 5: Estimation of the beam energy loss for the example pulse using BPM horizontal position measurements

4 Energy loss estimations using PETS forward power measurement and BPM intensity measurements

The TBTS provides direct measurement of the PETS output power, as well as the BPM intensity measurement, and we can therefore apply Eq. (7) directly to estimate the energy loss in the PETS. The locations of the PETS output forward measurements (diode) and the BPM intensity measurements used here to calculate Eq. (7) are shown in Figure 6.

Figure 7 shows, in red (o), the energy loss along the pulse estimated using the PETS output forward measurements and the BPM intensity measurements, $\langle U \rangle_{P_{meas}}$, for the pulse denoted "example pulse" in [5]. Analogous to the notation in [5] we use the suffix P_{meas} for estimations performed based on the PETS output forward measurements.

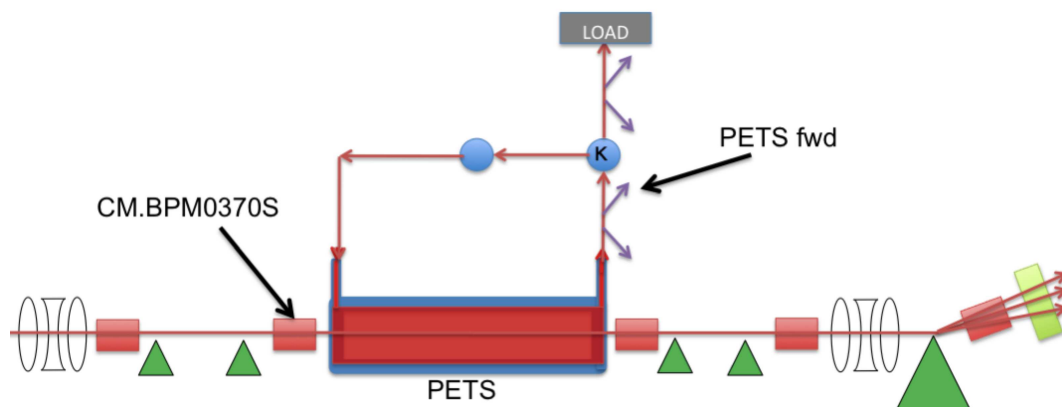


Figure 6: Location of the measurements used for estimating the beam energy loss from PETS forward power measurements and BPM intensity measurements

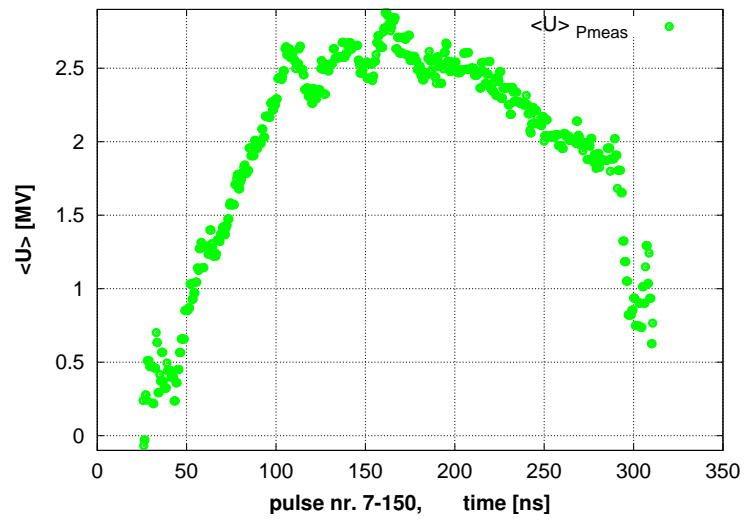


Figure 7: Estimation of the beam energy loss for the example pulse using PETS forward power measurements and BPM intensity measurements

5 Energy loss estimations using BPM intensity measurements alone

Using the system model described in [5] the total PETS output field, E , and power, P , can be reconstructed from the BPM intensity readings, and the energy loss can therefore be estimated using this measurement alone. We can then use Eq. (7) directly to estimate the energy loss. Alternatively, we could apply Eq. (4) using the reconstructed field. The locations of the BPM intensity measurements used here to calculate Eq. (7) are shown in Figure 8.

Figure 9 shows, in black (+), the energy loss along the pulse estimated using the BPM intensity measurement alone, $\langle U \rangle_{P_{mod}}$, for the pulse denoted "example pulse" in [5]. Analogous to the notation in [5] we use the suffix P_{mod} for estimations performed using the BPM intensity measurements alone, combined with the recirculation model.

Because the power scales with the square of the beam intensity while the voltage scales linearly with the beam intensity, erroneous BPM calibrations would result in scale error between $\langle U \rangle_{P_{mod}}$ and $\langle U \rangle_{P_{meas}}$.

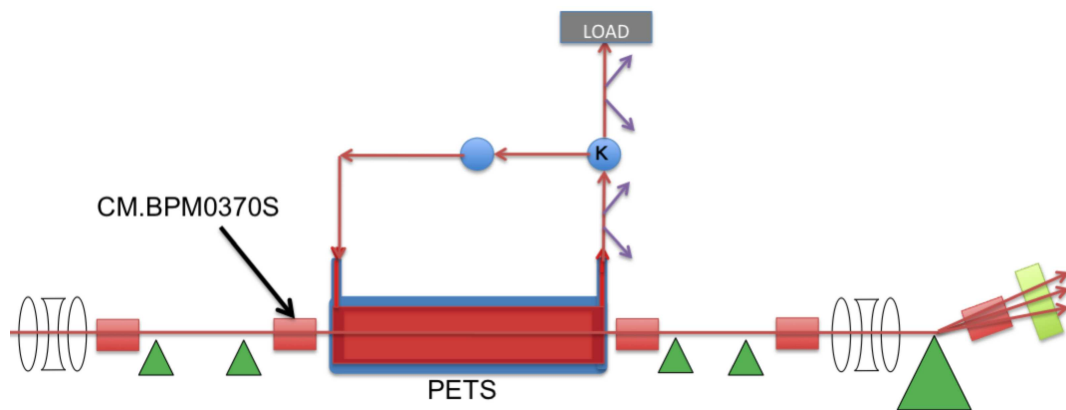


Figure 8: Location of the measurements used for estimating the beam energy loss from BPM intensity measurements alone

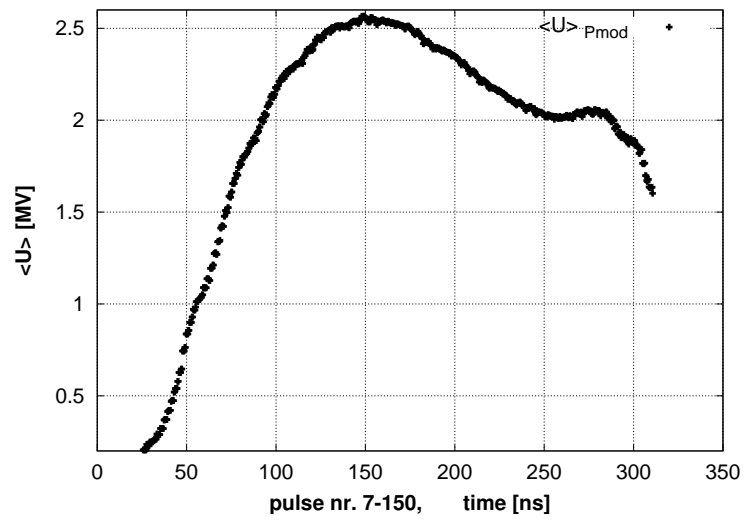


Figure 9: Estimation of the beam energy loss for the example pulse using BPM intensity measurements alone

6 Comparison between the three estimates

In this section we will compare the three different energy loss estimations for a number of pulses from the TBTS 2008 run. In Section 6.4 we will show statistics for a large number of pulses, however, we choose to present in full estimates for various pulse shapes and power levels. A subset of the pulses of which power measurements pulses which were already presented in [5] will therefore be shown.

In order to perform the comparison the estimations using the horizontal BPM readings, $\langle U \rangle_H$, have been offset so that the average of the peak part of the pulse corresponds to the average of the peak part of the estimations using the RF power readings, $\langle U \rangle_{Pmeas}$.

No artificial scaling has been applied to the estimates.

6.1 Comparison for the example pulse

We start by comparing the three estimations for the energy loss along the example pulse, already presented in Figures 5, 7 and 9.

In Figure 10 we have overlaid all three estimates in one graph $\langle U \rangle_H$, $\langle U \rangle_{Pmeas}$ and $\langle U \rangle_{Pmod}$. We also include the pulse intensity shape for reference. The energy loss comparison is performed for the time range where the intensity reading is above 1 A. Figure 11 shows for reference the PETS measured and reconstructed output power and the reconstructed and measured field phase, as already presented in [5] for the same pulse.

We observe good agreement between $\langle U \rangle_H$ and $\langle U \rangle_{Pmeas}$, although $\langle U \rangle_H$ also includes the effect of energy variation along the pulse entering the PETS. This might indicate that centroid energy variations along the incoming pulse are small (less than one percent), however this must be studied further before drawing final conclusions (by e.g. performing a direct measurement of the energy profile along the pulse, in CLEX upstream of the PETS).

Comparing $\langle U \rangle_{Pmod}$ with the other estimates, we see a good agreement at the first half of the pulse. Towards the second half there are some discrepancies that also show in the comparison between the reconstructed and the measured output power (in Figure 10, left). Towards the end of the pulse we also note that $\langle U \rangle_{Pmod}$ shows a significantly slower fall-off towards zero. The discrepancy here is more pronounced than in the power comparison. This effect is not fully understood yet, but it might be related to limited BPM bandwidth.

It should be noted that the relative timing of BPM signals and the RF signals has shifted with a few ns with respect to [5]. This was necessary in order to avoid blow up of $\langle U \rangle_{Pmeas}$ towards the end of the pulse.

6.2 Comparison for pulses without pulse shortening

We present a few pulses of different intensity profile, without pulse shortening. The first two pulses of the 15:48 series are shown in Figures 12 to 15.

Some high-power pulses with different intensity shape from the 16:02 series are shown in Figures 16 to 19.

We observe that for most parts the agreement between the three estimates is reasonable, but with discrepancies as already discussed in Section 6.1.

In Figure 18 there are some more discrepancies that might come from a non-ideal relative timing shift of the BPM and the RF signals.

6.3 Comparison for pulse with pulse shortening

For pulses where pulse shortening appears, probably due to break down, we do not expect the model with constant recirculation gain and phase to yield a good agreement for the energy loss estimations, analogous to the discrepancies between the measured and the reconstructed power, as discussed in [5].

The $\langle U \rangle_H$ measurement is using beam measurements only for the estimation and is independent of the recirculation model. $\langle U \rangle_H$ should therefore be considered the best reference for the actual beam energy loss in the beam during pulse shortening (eventual transverse break down kicks should also be identified by the least-squares technique, and should therefore not perturb the estimations of the energy loss).

Figure 20 shows the energy loss measurements for a shortened pulse, for which Figure 21 shows how the measured PETS output power starts to fall off rapidly around 200 ns, and apparently zero output is reached before the end of the pulse. From $\langle U \rangle_H$ we estimate that the beam energy loss falls gradually from when the pulse shortening starts after around 200 ns, until the end of the pulse after 300 ns. From $\langle U \rangle_{Pmeas}$ we observe a much faster fall of the estimated energy loss, and for a period of ~ 50 ns the energy loss is estimated to approximately zero. However, this is assuming a constant recirculation gain when applying Eq. (7). We did not see this plateau of zero energy loss for other pulses, so it might be that this effect is accidental.

Figure 22 shows the energy loss measurements of another shortened pulse. Figure 23 shows that for this pulse the measured PETS output power, as well as the estimated energy loss $\langle U \rangle_H$, reach zero at the same time as the beam intensity.

Figure 24 shows the energy loss measurements of a shortened pulse. For this pulse the real energy loss, $\langle U \rangle_H$, *increases* slightly after reaching a local minimum after pulse shortening. In the estimation based on Eq. (7), $\langle U \rangle_{Pmeas}$, we observe a voltage dip significantly into negative values, which would correspond to energy gain of the beam. While there is in principle nothing that rules out acceleration of the beam (neither in

the physics, nor in the model used here) the estimation $\langle U \rangle_H$ indicates that for this pulse there is no real acceleration of the beam. Scanning through a large number of pulses with break down shows no pulses where a clear beam acceleration is shown on $\langle U \rangle_H$.

By extending the system model with variable system parameters, eventually introducing new system parameters, one might seek to achieve good agreements between the different energy loss estimations. Letting a number of parameters vary freely, a good fit of both the PETS output power and the relative field phase have been obtained in [6]. Further checks could now be done by verifying the agreement of the energy loss estimations outlined in this note by applying models with varying parameters, but this is not pursued further in this note.

The quite different characteristic of the power and energy loss for the various pulses might be related to the location of eventual break downs (whether they occur in the PETS itself or in the wave guides, for example). However, for the data logged during the TBTS 2008 run there was no instrumentation available that could directly identify break down locations. In 2009 vibration sensors at the attenuator and the phase-shifter, as well as a camera monitoring the PETS will be installed for this purpose [10].

6.4 Statistics

In order to benchmark the agreement between the three estimation approaches, we apply them to a large number of pulses, and quantify the agreements. We choose to compare $\langle U \rangle_{Pmeas}$ to $\langle U \rangle_H$ and separately $\langle U \rangle_{Pmeas}$ to $\langle U \rangle_{Pmod}$. We define as metric for the difference of two estimates for a given pulse the following function

$$\varepsilon = \sqrt{\frac{\sum_{n=1}^N (\langle U \rangle_{Pmeas,n} - \langle U \rangle_{X,n})^2}{\sum_{n=1}^N (\langle U \rangle_{Pmeas,n})^2}}$$

where "X" stands for "H" or "Pmod". Summation is over each sample along the part of pulse where the intensity is above 1 A.

We apply this difference metric to the series of 200 pulses used to fit the recirculation parameters in [5], since it is a series where very little pulse shortening was observed. Pulses with low power (< 10 MW) corresponding to klystron problems were excluded in the histogram counts.

The results are shown in Figures 26 and 27. The 75% quartile of the distributions are 12.5 % and 16.6 % for the $\langle U \rangle_{Pmeas}, \langle U \rangle_H$ and the $\langle U \rangle_{Pmeas}, \langle U \rangle_{Pmod}$ comparison respectively. Comparing $\langle U \rangle_H$ and $\langle U \rangle_{Pmod}$ gave a 75 % quartile of 15.3 %.

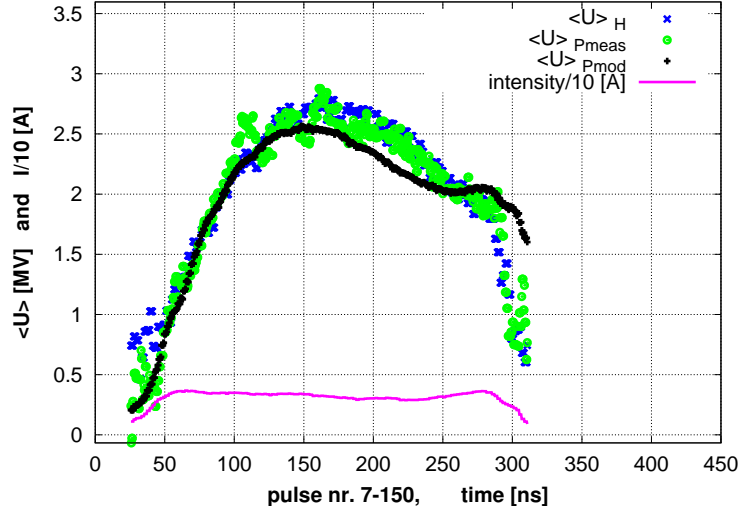


Figure 10: The example pulse. Energy loss estimates along the pulse based on BPM horizontal position measurements, $\langle U \rangle_H$, in blue (x), PETS forward diode power measurements and BPM intensity measurements, $\langle U \rangle_{Pmeas}$, in green (o) and BPM intensity measurements alone, $\langle U \rangle_{Pmod}$, in black (+). The BPM intensity is shown in magenta.

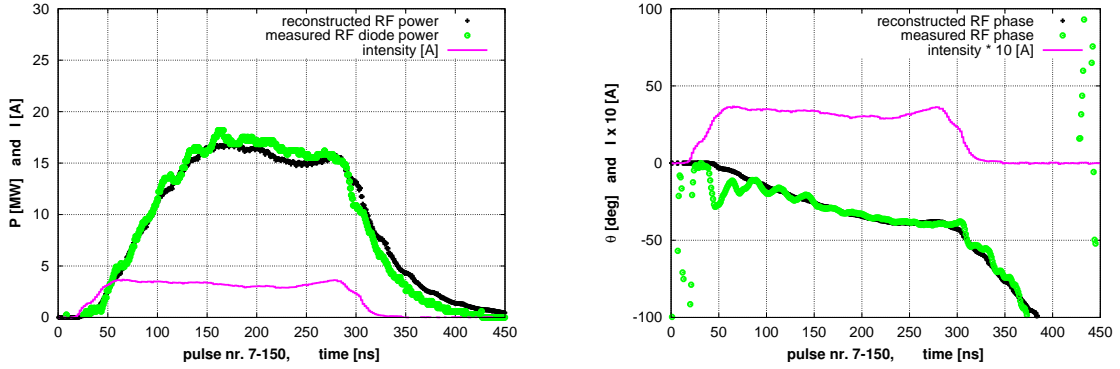


Figure 11: Power and phase for the pulse presented in Figure 10. Left: reconstructed and measured output RF power; reconstruction using the model in black (+) and diode power signal in green (o). Right: Reconstructed and measured relative field phase. Reconstruction using the model in black (+) and using the I&Q-channel measurements in green (o).

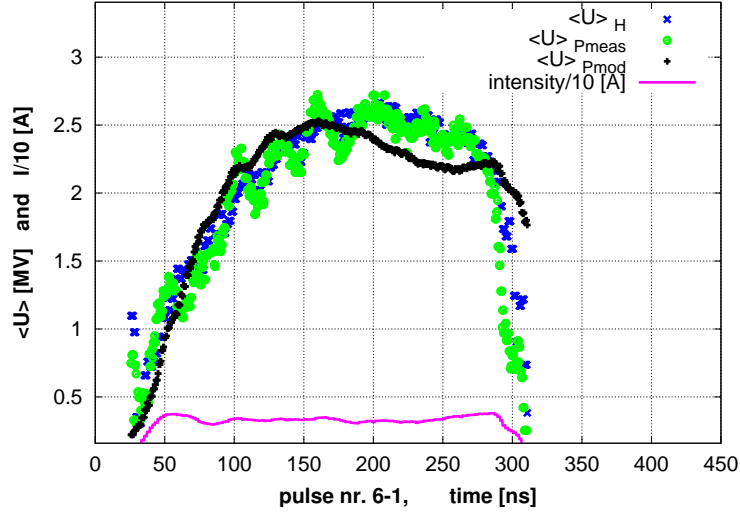


Figure 12: First pulse from the 15:48 series. Energy loss estimates along the pulse based on BPM horizontal position measurements, $\langle U \rangle_H$, in blue (x), PETS forward diode power measurements and BPM intensity measurements, $\langle U \rangle_{Pmeas}$, in green (o) and BPM intensity measurements alone, $\langle U \rangle_{Pmod}$, in black (+). The BPM intensity is shown in magenta.

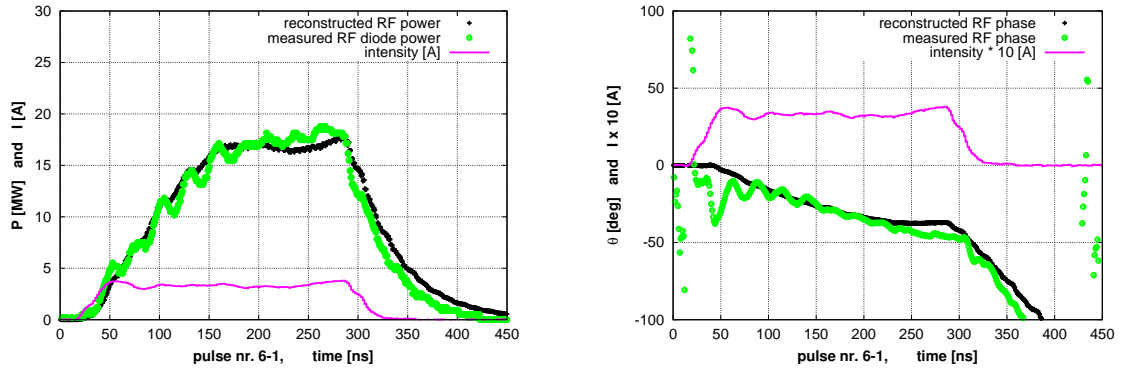


Figure 13: Power and phase for the pulse presented in Figure 12. Left: reconstructed and measured output RF power; reconstruction using the model in black (+) and diode power signal in green (o). Right: Reconstructed and measured relative field phase. Reconstruction using the model in black (+) and using the I&Q-channel measurements in green (o). The BPM intensity is shown in magenta.

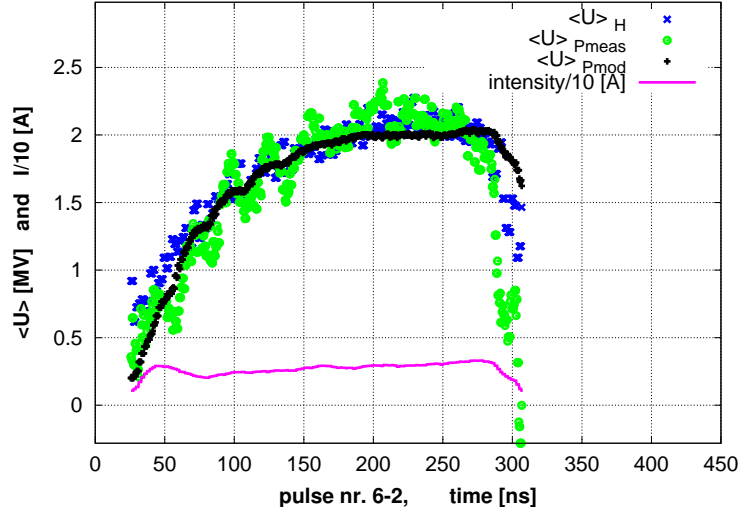


Figure 14: Second pulse from the 15:48 series. Energy loss estimates along the pulse based on BPM horizontal position measurements, $\langle U \rangle_H$, in blue (x), PETS forward diode power measurements and BPM intensity measurements, $\langle U \rangle_{P_{meas}}$, in green (o) and BPM intensity measurements alone, $\langle U \rangle_{P_{mod}}$, in black (+). The BPM intensity is shown in magenta.

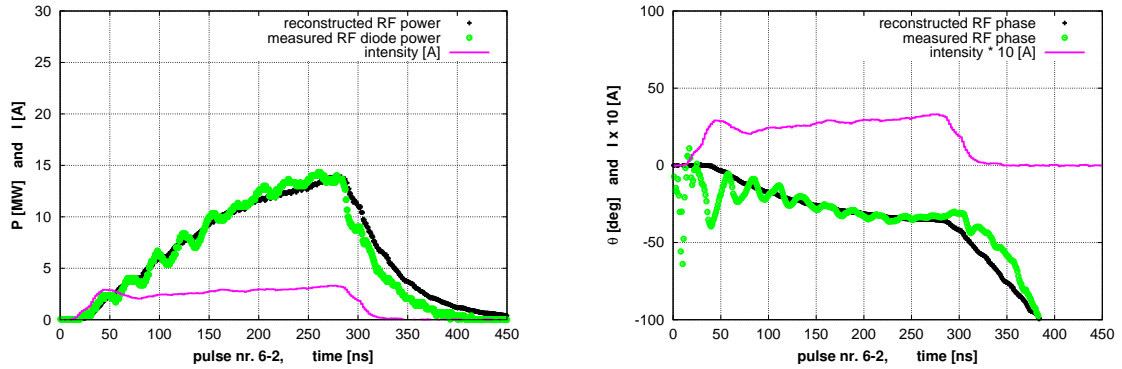


Figure 15: Power and phase for the pulse presented in Figure 14. Left: reconstructed and measured output RF power; reconstruction using the model in black (+) and diode power signal in green (o). Right: Reconstructed and measured relative field phase. Reconstruction using the model in black (+) and using the I&Q-channel measurements in green (o). The BPM intensity is shown in magenta.

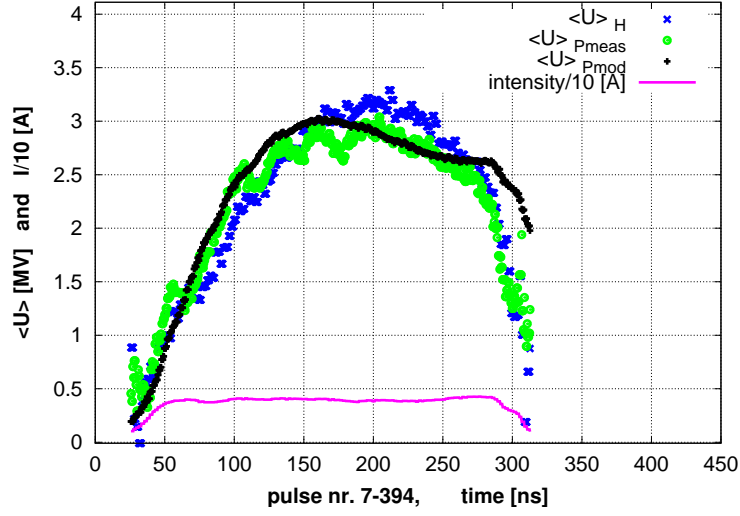


Figure 16: A high power, flat power top pulse from the 16:02 series. Energy loss estimates along the pulse based on BPM horizontal position measurements, $\langle U \rangle_H$, in blue (x), PETS forward diode power measurements and BPM intensity measurements, $\langle U \rangle_{Pmeas}$, in green (o) and BPM intensity measurements alone, $\langle U \rangle_{Pmod}$, in black (+). The BPM intensity is shown in magenta.

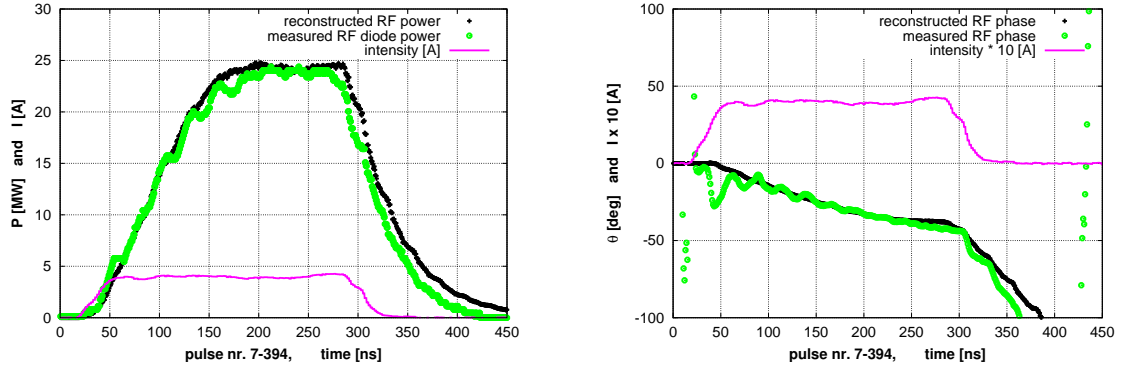


Figure 17: Power and phase for the pulse presented in Figure 16. Left: reconstructed and measured output RF power; reconstruction using the model in black (+) and diode power signal in green (o). Right: Reconstructed and measured relative field phase. Reconstruction using the model in black (+) and using the I&Q-channel measurements in green (o). The BPM intensity is shown in magenta.

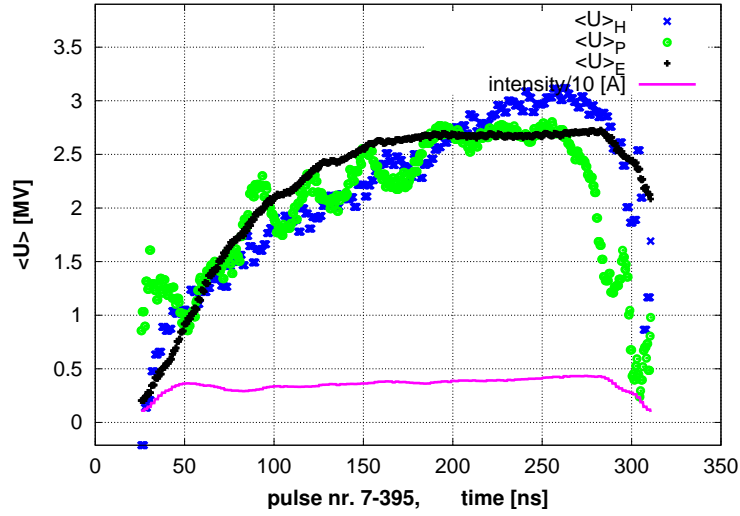


Figure 18: A high power, peaked power pulse from the 16:02 series. Energy loss estimates along the pulse based on BPM horizontal position measurements, $\langle U \rangle_H$, in blue (x), PETS forward diode power measurements and BPM intensity measurements, $\langle U \rangle_{Pmeas}$, in green (o) and BPM intensity measurements alone, $\langle U \rangle_{Pmod}$, in black (+). The BPM intensity is shown in magenta.

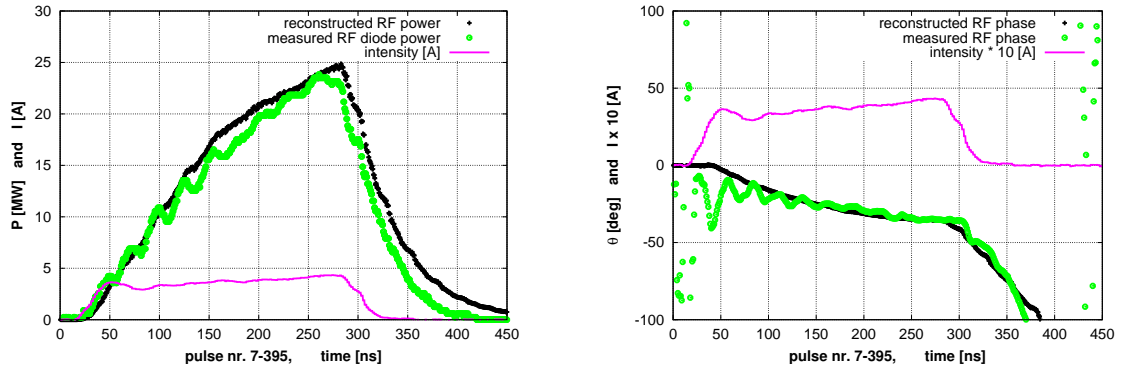


Figure 19: Power and phase for the pulse presented in Figure 18. Left: reconstructed and measured output RF power; reconstruction using the model in black (+) and diode power signal in green (o). Right: Reconstructed and measured relative field phase. Reconstruction using the model in black (+) and using the I&Q-channel measurements in green (o). The BPM intensity is shown in magenta.

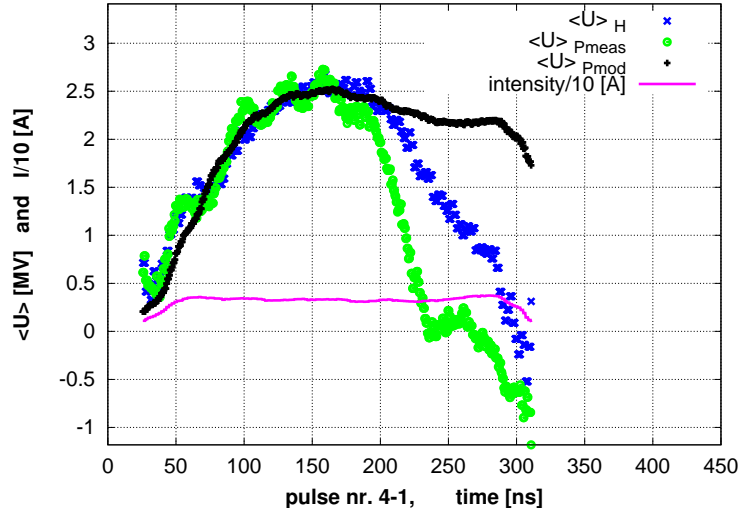


Figure 20: Pulse with pulse-shortening. The RF-power goes to zero before the end of the beam pulse. Energy loss estimates along the pulse based on BPM horizontal position measurements, $\langle U \rangle_H$, in blue (x), PETS forward diode power measurements and BPM intensity measurements, $\langle U \rangle_{Pmeas}$, in green (o) and BPM intensity measurements alone, $\langle U \rangle_{Pmod}$, in black (+). The BPM intensity is shown in magenta.

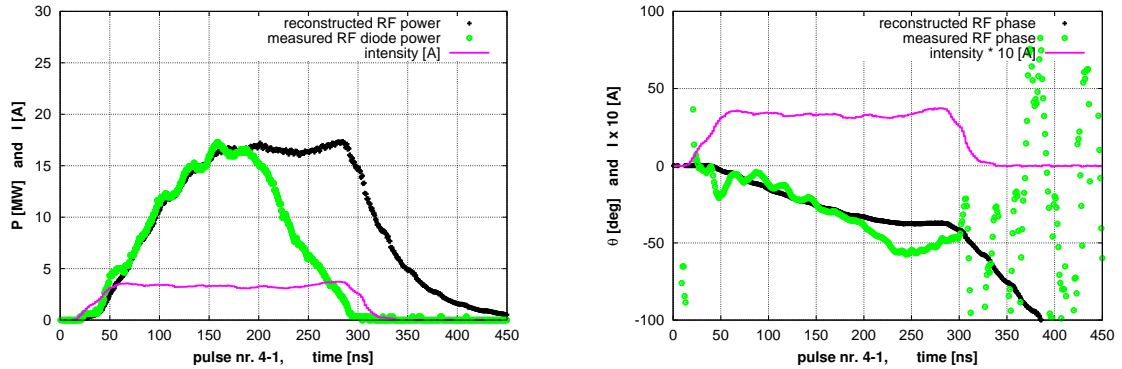


Figure 21: Power and phase for the pulse presented in Figure 20. Left: reconstructed and measured output RF power; reconstruction using the model in black (+) and diode power signal in green (o). Right: Reconstructed and measured relative field phase. Reconstruction using the model in black (+) and using the I&Q-channel measurements in green (o). The BPM intensity is shown in magenta.

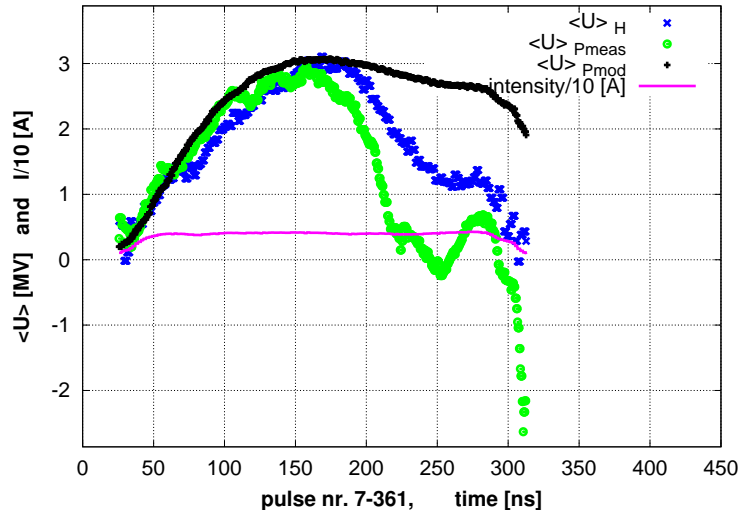


Figure 22: Pulse with pulse-shortening. The RF-power goes to zero at the same time as the beam intensity. Energy loss estimates along the pulse based on BPM horizontal position measurements, $\langle U \rangle_H$, in blue (x), PETS forward diode power measurements and BPM intensity measurements, $\langle U \rangle_{Pmeas}$, in green (o) and BPM intensity measurements alone, $\langle U \rangle_{Pmod}$, in black (+). The BPM intensity is shown in magenta.

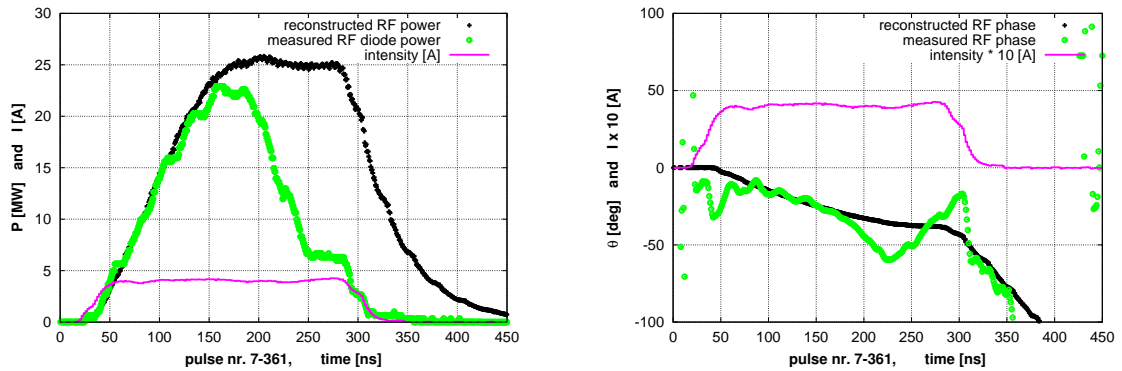


Figure 23: Power and phase for the pulse presented in Figure 22. Left: reconstructed and measured output RF power; reconstruction using the model in black (+) and diode power signal in green (o). Right: Reconstructed and measured relative field phase. Reconstruction using the model in black (+) and using the I&Q-channel measurements in green (o). The BPM intensity is shown in magenta.

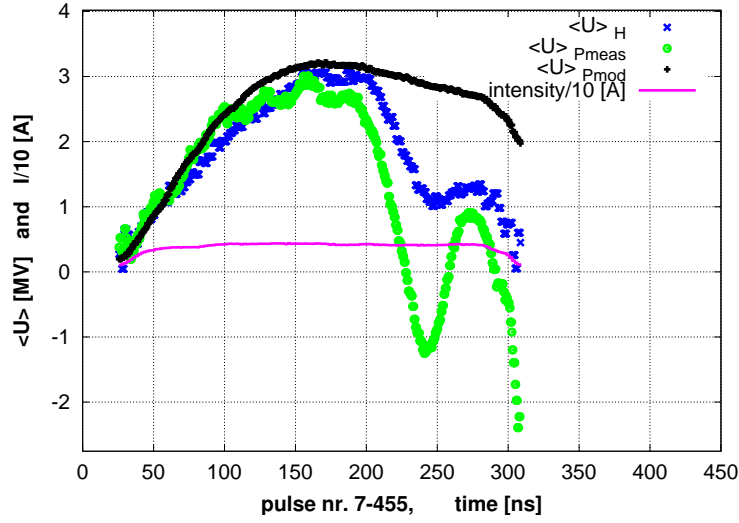


Figure 24: Pulse with pulse-shortening. The real energy loss, $\langle U \rangle_H$, increases slightly after reaching a local minimum after pulse shortening. Energy loss estimates along the pulse based on BPM horizontal position measurements, $\langle U \rangle_H$, in blue (x), PETS forward diode power measurements and BPM intensity measurements, $\langle U \rangle_{Pmeas}$, in green (o) and BPM intensity measurements alone, $\langle U \rangle_{Pmod}$, in black (+). The BPM intensity is shown in magenta.

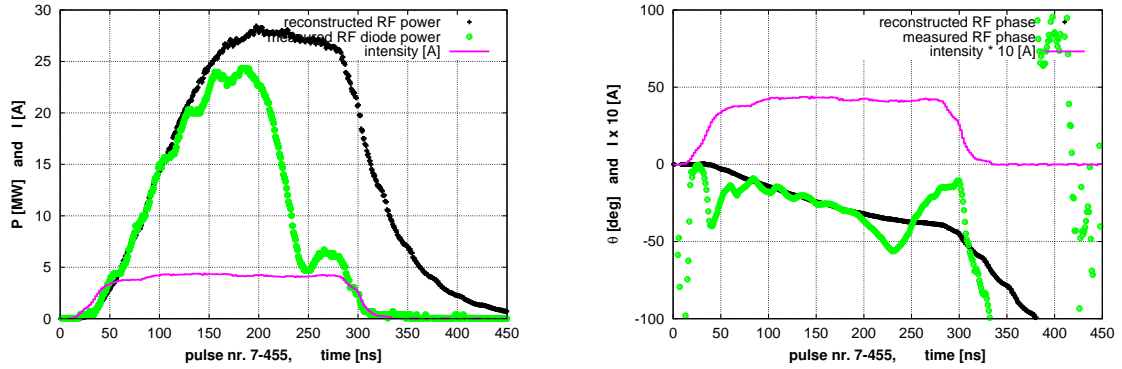


Figure 25: Power and phase for the pulse presented in Figure 24. Left: reconstructed and measured output RF power; reconstruction using the model in black (+) and diode power signal in green (o). Right: Reconstructed and measured relative field phase. Reconstruction using the model in black (+) and using the I&Q-channel measurements in green (o). The BPM intensity is shown in magenta.

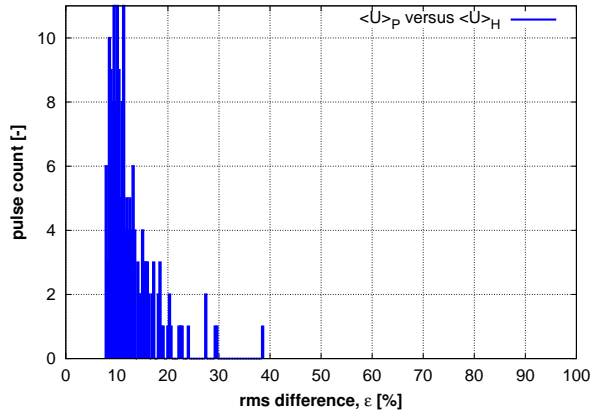


Figure 26: Rms difference, for a series of 200 pulses, of the estimates based on BPM horizontal position measurements compared with the estimates based on PETS forward diode power measurements and BPM intensity measurements

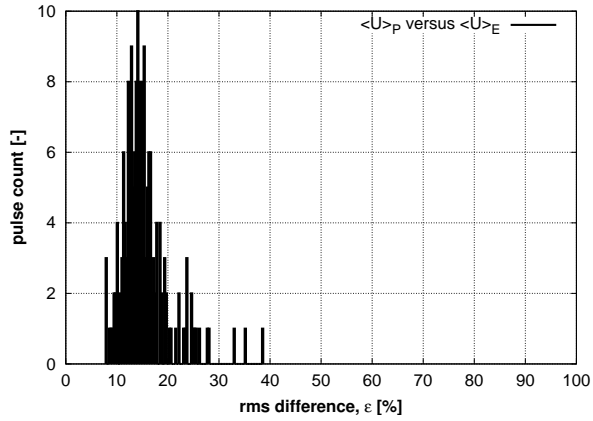


Figure 27: Rms difference, for a series of 200 pulses, of the estimates based on BPM intensity measurements alone compared with the estimates based on PETS forward diode power measurements and BPM intensity measurements

7 Conclusions

We have discussed the TBTS PETS beam energy loss, by using three different permutations of the available instrumentation combined with the simple model of recirculation described in [5].

The agreement between the three estimates is within 17 % for the 75 % quartile of the pulses investigated where no pulse shortening was observed.

For pulses where pulse shortening is observed the agreement is, as expected, no longer good, and more complicated models with varying system parameters, as e.g. investigated in [6], must be used to fit models and measurements. Such modelling might possibly bring new insight in the physics of break down, by comparing how parameters vary with respect to the constant-value models as e.g. presented in this note and [5].

However, in this note together with [5] we have shown how a simple model, in which the physics can be fully developed and understood by simple closed-form mathematical expressions, can explain both the PETS output power and the beam energy loss in the PETS with recirculation with a reasonable level of accuracy under nominal PETS operation.

7.1 Recommendations for future work

In order to precisely control and benchmark nominal PETS operation, and to do precision analysis for shortened pulses, it is of importance to increase further the precision of the estimates with respect to the results presented here.

Some suggestions for improvements are

- Taking into account measurements of incoming the beam centroid energy upstream of the PETS
- Improved data quality (measuring absolute values correct relative timing of the various measurement, calibration over the full range taking into account non-linearities, improving measurements bandwidth)
- Improved modelling using simulated wake functions and taking into account realistic beam-phases (discussed further in [5])

8 Acknowledgements

Useful discussions with Roger Ruber, Volker Ziemann, Daniel Schulte and Igor Syrathev are gratefully acknowledged, and special thanks to Roger Ruber for careful proof-reading.

References

- [1] I. Syratchev et al., High RF Power Production for CLIC, *CERN CLIC Note 720 and Proceedings of PAC'07*, WEPMN071 (2007)
- [2] R.J.M.Y. Ruber et al., The CTF3 Two-Beam Test-Stand Installation and Experimental Program, *Proceeding of EPAC'08*, WEPP139 (2008)
- [3] G. Geschonke, A. Ghigo (ed.) et al., "CTF3 Design Report", CERN/PS 2002-008(RF), LNF-02/008(IR).
- [4] I. Syratchev et al., CLIC RF High Power Production Testing Program, *Proceeding of EPAC'08*, WEOBG01 (2008)
- [5] E. Adli, Analysis of the first 12 GHz PETS tests with beam using a constant parameter recirculation model, *CERN CTF3 Note 096* (2009)
- [6] V. Ziemann, Data Analysis for PETS Recirculation, CERN CTF3 Note 094 (2009)
- [7] M. Johnson, Beam-Based Diagnostics of RF-breakdown in the Two-Beam test-stand in CTF3, *CERN CLIC Note 710* (2007)
- [8] M. Johnson and R. Ruber, MAD-X input files for the CTF3 Two-beam Test-stand drive beam line. CERN EDMS document 903028 version 3, <https://edms.cern.ch/document/903028/3> (2008)
- [9] Simona Bettoni, private communication
- [10] Roger Ruber, private communication